Band terminations in the nucleus ^{46}Ti

D. Bucurescu,[1] C. A. Ur,[1,2] S. M. Lenzi,[2] D. R. Napoli,[3] J. Sánchez-Solano,[4] D. Bazzacco,[2] F. Brandolini,[2] G. de Angelis,[3] E. Farnea,[2] A. Gadea,[3] S. Lunardi,[2] N. Mărginean,[1,3] Zs. Podolyak,[5] A. Poves,[4] and C. Rossi Alvarez[2]

[1]*H. Hulubei Institute of Physics and Nuclear Engineering, R-76900 Bucharest, Romania*

[2]*Dipartimento di Fisica and INFN, Sezione di Padova, I-35131 Padova, Italy*

[3]*Laboratori Nazionali di Legnaro, INFN, I-35020 Legnaro, Italy*

[4]*Department de Fisica Teórica C–XI, Universidad Autónoma de Madrid, E-28049 Madrid, Spain*

[5]*Department of Physics, University of Surrey, Guilford GU2 7XH, United Kingdom*

(Received 28 October 2002; published 18 March 2003)

High-spin states in ^{46}Ti have been investigated with the reaction ^{28}Si(^{24}Mg,$\alpha 2p$) at 100 MeV, using the GASP γ-ray array and the charged-particle detector ISIS. The positive parity yrast sequence has been observed up to the 14^+ terminating state and several high-energy transitions have been established above the termination state. Both the signatures of a negative parity band have been observed up to the 16^- and 17^- terminating states, plus one more transition from an 18^- state at 19.086 MeV excitation. The observed states are interpreted within the frame of large scale shell model calculations in the full pf space (positive parity) and as particle-hole excitations from the $d_{3/2}$ shell (negative parity).

DOI: 10.1103/PhysRevC.67.034306 PACS number(s): 21.10.Tg, 21.60.Cs, 23.20.Lv, 27.40.+z

I. INTRODUCTION

The nuclei in the $1f_{7/2}$ shell have become a recognized laboratory source in which our understanding of the interplay between collective behavior and shell model effects can be studied in great detail. Theoretically, this has become possible due to large scale shell model calculations performed in the full pf shell [1]. Experimentally, the highly efficient γ-ray detector arrays made it possible to study these nuclei at relatively high spins, up to configuration terminating states or even higher, where the structure is dominated by the alignment of all the valence nucleons, as well as excitations of the core. Many band terminations have been observed in these nuclei for the natural parity states [2], while for the non-natural bands, they have been observed only in a few cases: ^{44}Ti [3], ^{45}Sc [4], ^{46}V [5], ^{47}V [6].

This paper presents new experimental results on high-spin states for the ^{46}Ti nucleus. This nucleus is close to ^{48}Cr, which is the $f_{7/2}$-shell nucleus with the largest valence particle number and therefore the most collective. Low-spin states in ^{46}Ti have been studied by means of β-decay and different light particle induced reactions [7,8]. High-spin states have been observed through heavy-ion fusion-evaporation reactions up to the termination of the positive parity yrast sequence [9–11].

In the present work, we follow both the positive (natural) parity and negative (non-natural) parity state sequences above their terminations. In total, 20 new levels with spin above $10\hbar$ and excitation energy higher than 8 MeV have been established in this nucleus. These experimental results are compared with full pf shell model calculations, as well as calculations which allow for particle-hole excitations involving the $1d_{3/2}$ orbital.

II. EXPERIMENTS AND RESULTS

A. Experimental details

The data containing information on the high-spin states of ^{46}Ti have been obtained from an experiment where the target was a self-supported 0.4 mg/cm^2 foil of 99.99% enriched ^{28}Si and the beam was ^{24}Mg at 100 MeV [12], with ^{46}Ti being populated by the $\alpha 2p$ channel.

The beam was delivered by the XTU Tandem accelerator of the National Laboratories of Legnaro. The γ rays were detected with the GASP array [12] that consists of 40 HP Ge detectors of high efficiency, with anti-Compton shields, and an inner ball (multiplicity filter) of 80 BGO elements. Detection and identification of light charged particles from the reactions were made with the ISIS silicon ball [13] that consists of 40 ΔE-E Si telescopes with a geometry similar to that of the GASP Ge detectors. Events were collected on tape if at least two Ge detectors and two BGO elements of the inner ball fired in coincidence. A total of 7.0×10^8 twofold and 7.3×10^7 threefold events were collected. The γ rays were recorded up to an energy of 6.5 MeV.

B. Data analysis and the level scheme

The average recoil velocity of the ^{46}Ti nuclei was about $0.044c$ and a simple Doppler correction with this value led to rather broad peaks (e.g., about 12 keV full width at half maximum at 1.5 MeV), an effect mainly due to the evaporation of high-energy α particles. By using the information from the ISIS detector on the geometry of the evaporated particles, one could apply an event-by-event kinematic correction [14], thus improving by 25% the resolution of the γ-ray spectra (i.e., about 9 keV at 1.5 MeV).

The data were sorted in symmetrized γ-γ and γ-γ-γ coincidence matrices, both with or without conditions on the ISIS data. By observing the coincidence relationships and relative intensities of the transitions, we have built the level scheme shown in Fig. 1. Several examples of double-gated spectra related to this level scheme are shown in Fig. 2.

Table I contains information concerning the intensities and multipolarities of all the transitions in Fig. 1. The transition multipolarities have been deduced on the basis of di-

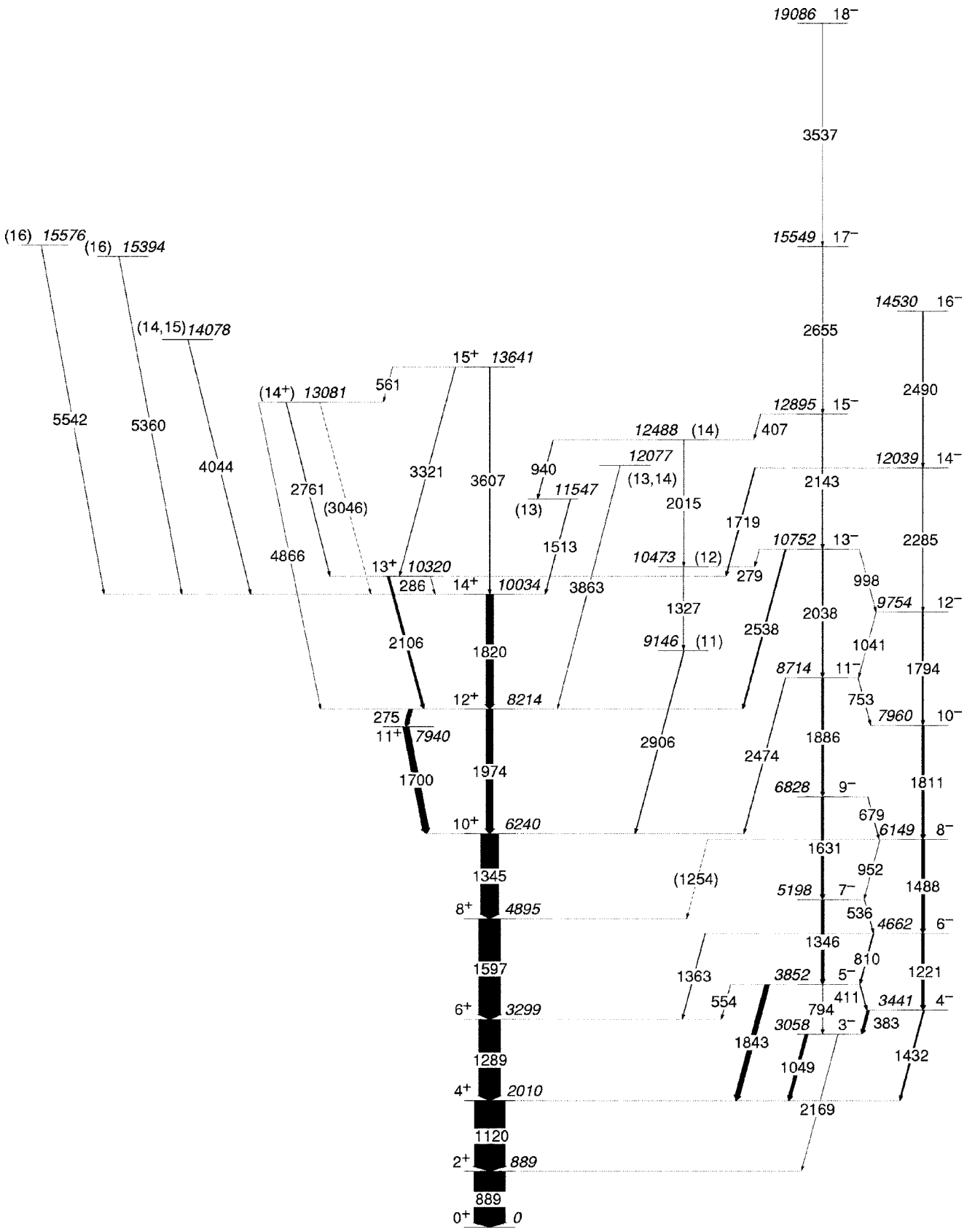

FIG. 1. The level scheme of the ^{46}Ti nucleus as resulted from the present experiments. The widths of the arrows are proportional to the relative intensities of the γ-ray transitions (Table I).

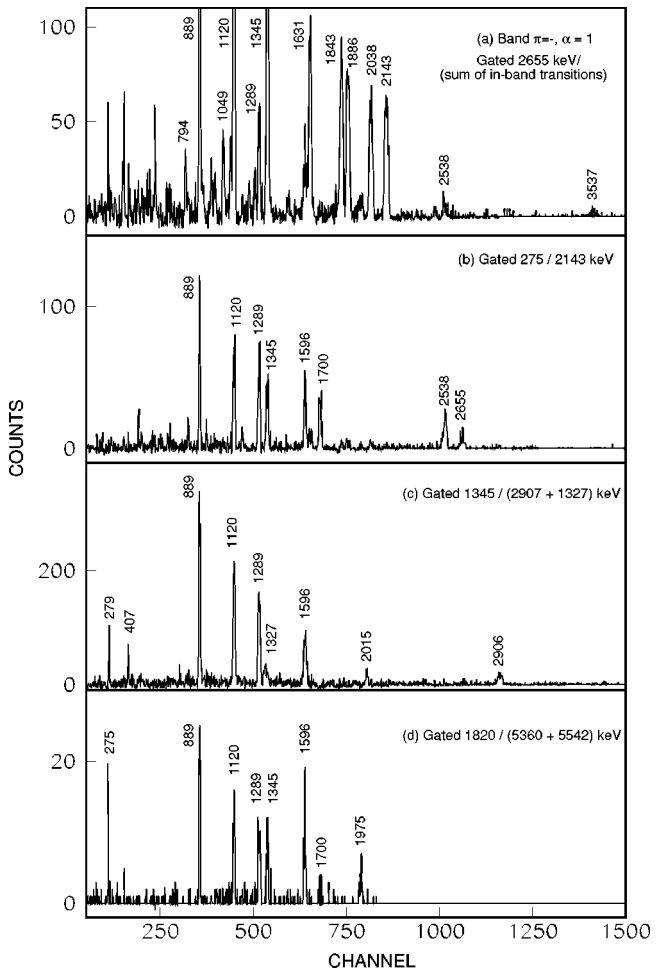

FIG. 2. Double-gated γ-ray coincidence spectra cut from a γ-γ-γ coincidence cube. The two gates (or sum of gates) are indicated in each case. Spectrum (a) illustrates one of the negative parity bands; (b) highlights one of the connections of the negative parity band with the yrast positive parity band; (c) shows the cascade of three transitions feeding the 10^+ level; (d) the feeding of the yrast positive parity band above the 14^+ state by the highest-energy transitions observed, of about 5.5 MeV.

rectional correlation from oriented states (DCO) ratios [15] and on the angular distributions of the γ rays [16]. The DCO ratios were calculated as

$$R_{DCO}=\frac{I_{\gamma_1}(\theta_1;\ \text{gated by}\ \ \gamma_2\ \ \text{at}\ \ \theta_2)}{I_{\gamma_1}(\theta_2;\ \text{gated by}\ \ \gamma_2\ \ \text{at}\ \ \theta_1)},$$

gate is set on the γ_2 transition. They have been determined from asymmetric γ-γ matrices which had on one axis the γ rays from the 90° ring of detectors and on the other one those from the 35° and 145° rings of detectors. Such matrices have been obtained in coincidence either with one proton, or with one α particle. In our case, for $\theta_1=90°$ and $\theta_2=35°$ and 145°, gating on a stretched quadrupole transition γ_2, one gets for R_{DCO} a value of $\sim$1.0 if the γ_1 transition is a stretched quadrupole, or $\sim$0.5 if it is a stretched pure dipole one. By gating on a stretched pure dipole transition, one should get $\sim$2.0 for a quadrupole and $\sim$1.0 for a pure dipole transition. For mixed dipole/quadrupole γ_2 transitions, R_{DCO} depends on the δ value.

We have built also seven asymmetric γ-γ matrices corresponding to the coincidence of the detectors from each ring of GASP (35°, 60°, 72°, 90°, 108°, 120°, and 145°) with the rest of all the other detectors; these matrices were also coincident with charged particles. Clean γ-ray spectra were obtained from these matrices by gating on the all-detector axis, on a number of ^{46}Ti transitions, and they were corrected for the efficiency of the corresponding ring of detectors. Since the GASP array has many detectors, placed at many different angles, the angular correlation effects between any two γ rays are washed out, so that the intensity of any γ ray in the seven rings does not depend on the character of the gating transition(s), but follows the regular angular distribution of γ rays from oriented nuclei [16].

The experimental values A_2/A_0 and A_4/A_0 resulting from a Legendre polynomial analysis of the angular distributions, and/or the R_{DCO} value are given in Table I for most of the observed transitions. These two sets of data are rather consistent with each other and support the assignments shown in Fig. 1 and on the last column of Table I. In some cases, the transitions consistent with a dipole or quadrupole type have been assumed as of $M1$ or $E2$ mutipolarity, respectively, as suggested by the observed decay patterns, while in some others no parity assignment was made.

As in a recent heavy-ion in-beam investigation [11], we assign to the 1820 keV γ ray in the positive parity yrast sequence a quadrupole character, and therefore assume that it is a $14^+\rightarrow12^+$ transition. The 14^+ state is actually the terminating state having the maximum spin available to ^{46}Ti in a pure $f_{7/2}$-shell configuration. The yrast sequence continues above the 14^+ terminating state with one transition of high energy (3.6 MeV), which is of dipole type (Table I), and it is therefore assigned to the decay of a 15^+ state. Above the 12^+ state at $E_x=8.214$ MeV [7,8,11], the observed level scheme is rather complex and presents many levels which deexcite mainly by high-energy transitions. Most of the transitions feeding the 12^+ and 14^+ yrast states are of dipole character. Exception are two very high-energy transitions (5.36 and 5.54 MeV) which feed the 14^+ state and appear to be of quadrupole character (Table I), therefore likely to deexcite 16^+ states.

The states with excitation energies of 10.320 MeV and 13.081 MeV have been assigned positive parity on the basis of their connections with the positive parity yrast band. For the states at 9.146, 10.473, 11.547, 12.077, and 12.488 MeV, tentative spin assignments have been made (see Fig. 1), but since they also have connections with negative parity states (see below), no definite parity assignment is proposed.

Two regular band structures built on the states 3^- (3.058 MeV) and 4^- (3.441 MeV) and interpreted as the signature partners of a rotational negative parity band were previouslyknown up to the spins 9^- and 8^-, respectively [7,8]. Such

TABLE I. γ-ray intensities, DCO ratios, Legendre polynomial coefficients of the angular distributions, and the tentative spin-parity assignments for ^{46}Ti levels and transitions.

E_γ (keV)	Intensities	DCO ratios[a]	A_2/A_0[b]	A_4/A_0[b]	Assignment
275.2	13.5(1)	0.70(5)	−0.38(13)	−0.57(21)	$12_1^+ \rightarrow 10_1^+$
279.3	0.40(5)				$13_1^- \rightarrow (12)$
286.2	0.30(6)	0.60(15)			$13_1^+ \rightarrow 14_1^+$
382.9	8.5(1)	1.38(4)	0.22(4)	−0.18(10)	$4_1^- \rightarrow 3_1^-$
407.2	~0.6				$15_1^- \rightarrow (14)$
410.9	1.1(2)	0.94(13)	−0.18(7)	−0.32(12)	$5_1^- \rightarrow 4_1^-$
535.9	0.8(1)	0.9(2)			$7_1^- \rightarrow 6_1^-$
553.6	0.6(1)				$5_1^- \rightarrow 6_1^+$
560.5	0.30(5)	0.57(20)	−0.43(10)	−0.09(16)	$15_1^+ \rightarrow (14_2^+)$
678.5	1.0(1)				$9_1^- \rightarrow 8_1^+$
753.0	0.5(1)				$11_1^- \rightarrow 10_1^-$
793.8	1.9(2)	0.95(17)	0.24(13)	−0.09(23)	$5_1^- \rightarrow 3_1^-$
809.8	2.9(1)	1.3(2)	0.63(8)	0.20(15)	$6_1^- \rightarrow 5_1^-$
889.2	100.0(10)		0.09(10)	−0.15(14)	$2_1^+ \rightarrow 0_1^+$
940.0	1.6(1)	0.76(12)	−0.54(9)	0.06(19)	$(14) \rightarrow (13)$
952.1	0.4(1)				$8_1^- \rightarrow 7_1^-$
998.0	0.13(4)				$13_1^- \rightarrow 12_1^-$
1040.7	0.10(5)				$12_1^- \rightarrow 11_1^-$
1048.7	10.0(4)	0.97(4)	−0.08(8)	−0.05(13)	$3_1^- \rightarrow 4_1^+$
1120.4	97.3(25)	0.97(3)			$4_1^+ \rightarrow 2_1^+$
1220.6	9.2(2)	0.91(5)	0.18(8)	−0.11(12)	$6_1^- \rightarrow 4_1^-$
(1254)					$8_1^- \rightarrow 8_1^+$
1289.0	68.9(12)	1.03(4)	0.19(12)	−0.15(15)	$6_1^+ \rightarrow 4_1^+$
1327.0	1.2(1)	0.30(8)	−0.48(11)	−0.20(24)	$(12) \rightarrow (11)$
1345.0	57.1(5)	0.97(4)	0.22(7)	−0.16(14)	$10_1^+ \rightarrow 8_1^+$
1345.5	8.6(2)	1.03(4)	0.17(15)	−0.21(25)	$7_1^- \rightarrow 5_1^-$
1363.1	1.6(1)	1.1(2)			$6_1^- \rightarrow 6_1^+$
1431.7	4.5(3)	0.90(9)	−0.08(6)	−0.02(13)	$4_1^- \rightarrow 4_1^+$
1487.5	10.5(3)	0.98(8)	0.19(8)	−0.18(16)	$8_1^- \rightarrow 6_1^-$
1512.7	1.6(1)	0.38(12)	−0.28(8)	−0.07(10)	$(13) \rightarrow 14_1^+$
1596.5	68.4(15)	0.98(2)	0.19(8)	−0.15(13)	$8_1^+ \rightarrow 6_1^+$
1630.6	8.0(4)	1.19(4)	0.12(7)	−0.15(14)	$9_1^- \rightarrow 7_1^-$
1699.5	20.3(8)	0.50(2)	−0.40(5)	−0.06(12)	$11_1^+ \rightarrow 10_1^+$
1719.0	2.8(2)	0.50(6)	−0.05(11)	0.02(20)	$14_1^- \rightarrow 13_1^+$
1794.0	3.8(4)	0.87(11)	0.28(11)	−0.06(19)	$12_1^- \rightarrow 10_1^-$
1811.2	7.7(4)	0.95(9)	0.26(9)	−0.14(15)	$10_1^- \rightarrow 8_1^-$
1820.1	25.2(6)	0.95(4)	0.21(8)	−0.14(13)	$14_1^+ \rightarrow 12_1^+$
1842.6	15.4(2)	0.7(5)	−0.27(7)	−0.04(11)	$5_1^- \rightarrow 4_1^+$
1885.6	5.7(3)	1.06(6)	0.17(7)	−0.16(13)	$11_1^- \rightarrow 9_1^-$
1974.2	23.5(5)	1.04(4)	0.22(9)	−0.12(14)	$12_1^+ \rightarrow 10_1^+$
2014.7	1.10(6)	0.97(15)	0.39(15)	−0.14(32)	$(14) \rightarrow (12)$
2038.4	4.3(1)	1.04(5)	0.23(12)	−0.25(22)	$13_1^- \rightarrow 11_1^-$
2106.2	7.1(2)	0.60(15)	−0.26(6)	−0.07(12)	$13_1^+ \rightarrow 12_1^+$
2142.7	2.9(1)	0.98(6)	0.22(5)	−0.12(9)	$15_1^- \rightarrow 13_1^-$
2169.0	0.26(4)				$3_1^- \rightarrow 2_1^+$
2285.0	1.0(1)	0.77(16)	0.38(16)	−0.31(26)	$14_1^- \rightarrow 12_1^-$
2452.3	1.4(1)	1.24(23)	0.34(9)	−0.36(9)	$(14) \rightarrow 14_1^+$
2474.0	1.8(2)	0.31(10)			$11_1^- \rightarrow 10_1^+$
2490.2	1.9(1)	0.82(23)	0.18(13)	−0.37(21)	$16_1^- \rightarrow 14_1^-$
2537.7	4.0(8)	0.42(7)	−0.36(9)	0.03(14)	$13_1^- \rightarrow 12_1^+$
2654.5	1.6(1)	0.83(12)	0.09(9)	−0.17(15)	$17_1^- \rightarrow 15_1^-$

TABLE I. (*Continued*).

E_{gg} (keV)	Intensities	DCO ratios[a]	A_2/A_0[b]	A_4/A_0[b]	Assignment
2760.5	1.1(2)	0.60(12)	0.14(16)	0.26(39)	$(14_2^+)\rightarrow 13_1^+$
2906.2	1.9(1)	0.55(9)	−0.49(9)	−0.28(16)	$(11)\rightarrow 10_1^+$
(3046)					$(14_2^+)\rightarrow 14_1^+$
3321	1.0(2)	1.4(4)			$15_1^+\rightarrow(13_1^+)$
3537	0.24(5)		−0.83(13)	0.09(20)	$18_1^-\rightarrow 17_1^-$
3607	2.2(1)	0.28(7)	−0.67(14)	0.53(22)	$15_1^+\rightarrow 14_1^+$
3863	0.6(1)		−0.14(19)	−0.42(30)	$(13,14)\rightarrow 12_1^+$
4044	∼0.8	0.31(15)	−0.17(18)	0.05(32)	$(14,15)\rightarrow 14_1^+$
4866	0.4(1)	1.9(5)[c]			$(14_2^+)\rightarrow 12_1^+$
5360	∼0.5	0.91(36)			$(16)\rightarrow 14_1^+$
5542	∼0.5	1.12(33)			$(16)\rightarrow 14_1^+$

[a]From gate set on a quadrupole transition.
[b]Angular distribution Legendre polynomial coefficients.
[c]From gate set on the dipole transitions 275 and 1700 keV.

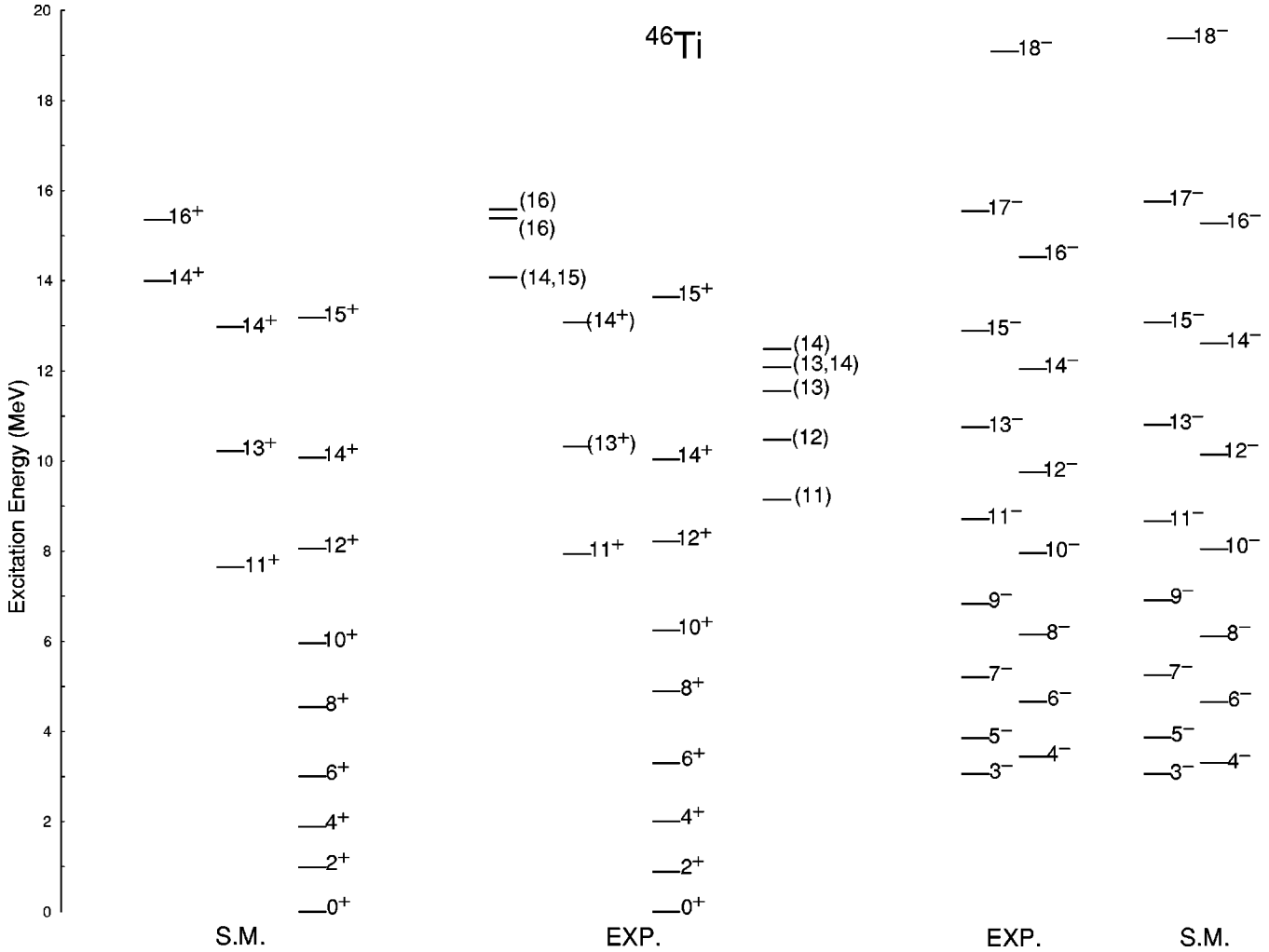

FIG. 3. Comparison between the experimental level scheme of ^{46}Ti and the one calculated with the shell model (code ANTOINE), in the full pf shell. For the experimental levels without parity assignment, no possible theoretical counterparts are shown.

TABLE II. Comparison between experimental and shell model values for branching ratios in ^{46}Ti. The calculated values take in account the predicted $M1+E2$ admixture for the $\Delta J=1$ transitions.

E_x (keV)	Assignment	Transition	E_y (keV)	Branch Expt.	Branch Calc.
		Positive parity levels			
8214	12_1^+	$12_1^+ \rightarrow 11_1^+$	275	57.4(12)	51.49
		$12_1^+ \rightarrow 10_1^+$	1974	100(2)	100.00
10320	13_1^+	$13_1^+ \rightarrow 14_1^+$	286	4.2(8)	8.03
		$13_1^+ \rightarrow 12_1^+$	2106	100(3)	100.00
13081	14_2^+	$14_2^+ \rightarrow 14_1^+$	3046		30.76
		$14_2^+ \rightarrow 13_1^+$	2761	100(18)	100.00
		$14_2^+ \rightarrow 12_1^+$	4866	36(11)	30.95
13641	15_1^+	$15_1^+ \rightarrow 14_1^+$	3607	100(5)	100.00
		$15_1^+ \rightarrow 13_1^+$	3321	46(9)	25.73
		Negative parity levels			
3852	5^-	$5^- \rightarrow 4^-$	411	58(8)	100.00
		$5^- \rightarrow 3^-$	794	100(10)	79.28
4662	6^-	$6^- \rightarrow 5^-$	810	31.5(13)	90.25
		$6^- \rightarrow 4^-$	1221	100(2)	100.00
5198	7^-	$7^- \rightarrow 6^-$	536	9.3(12)	13.20
		$7^- \rightarrow 5^-$	1346	100(2)	100.00
6149	8^-	$8^- \rightarrow 7^-$	952	3.8(10)	44.50
		$8^- \rightarrow 6^-$	1488	100(3)	100.00
6828	9^-	$9^- \rightarrow 8^-$	679	12.5(14)	9.39
		$9^- \rightarrow 7^-$	1631	100(5)	100.00
7960	10^-	$10^- \rightarrow 9^-$	1132		12.48
		$10^- \rightarrow 8^-$	1811	100	100.00
8714	11^-	$11^- \rightarrow 10^-$	753	8.8(18)	2.03
		$11^- \rightarrow 9^-$	1886	100(5)	100.00
9754	12^-	$12^- \rightarrow 11^-$	1041	2.6(13)	4.77
		$12^- \rightarrow 10^-$	1794	100(11)	100.00
10752	13^-	$13^- \rightarrow 12^-$	998	3.0(9)	11.49
		$13^- \rightarrow 11^-$	2038	100(2)	100.00
12039	14^-	$14^- \rightarrow 13^-$	1287		100.00
		$14^- \rightarrow 12^-$	2285	100	29.16
12895	15^-	$15^- \rightarrow 14^-$	856		100.00
		$15^- \rightarrow 13^-$	2143	100	43.49
14530	16^-	$16^- \rightarrow 15^-$	1635		10.25
		$16^- \rightarrow 14^-$	2490	100	100.00
15549	17^-	$17^- \rightarrow 16^-$	1019		0.39
		$17^- \rightarrow 15^-$	2655	100	100.00
19086	18^-	$18^- \rightarrow 17^-$	3537	100	100.00
		$18^- \rightarrow 16^-$	4556		17.08

a non-natural parity band can be described within the shell model, as a particle-hole excitation from the closed $d_{3/2}$ shell. The terminating states of the $\alpha=0$ and $\alpha=1$ signature bands are, in this picture, 16^- and 17^-, respectively. We have observed for the first time, in the present experiments, the two signature bands up to their termination. In addition, a higher transition of 3.54 MeV, which feeds the terminating state of the $\alpha=1$ band is reported.

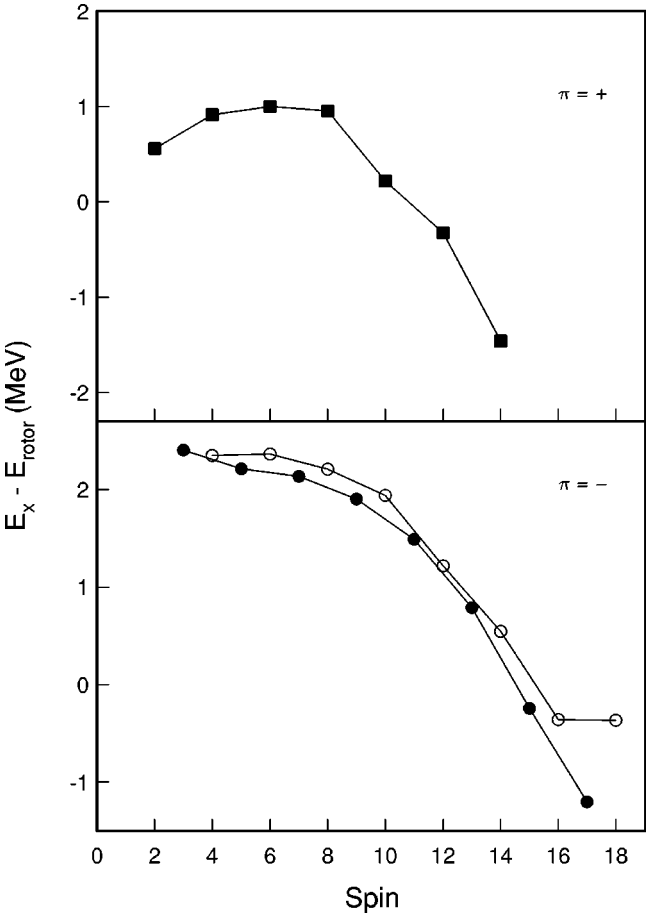

FIG. 4. Comparison of the positive parity yrast band and the negative parity bands with a rotor formula $E(J)=32.32A^{-5/3}J(J+1)$.

III. COMPARISON WITH SHELL MODEL: CALCULATIONS AND DISCUSSION

As stated in the Introduction, shell model calculations in the full pf space give a very good description of the structure of $f_{7/2}$-shell nuclei. We have therefore compared the present experimental data to predictions of such calculations. To account for negative parity states, a particle-hole excitation from the $d_{3/2}$ shell has been considered. These calculations have been performed with the code ANTOINE [17], using the KB3 interaction and experimental single-particle energies from ^{41}Ca [1]. The results for ^{46}Ti are shown in Fig. 3.

The positions of the positive parity yrast states up to the 15^+ state (above the band termination) are well reproduced. Table II shows the calculated and experimental branching ratios for the higher-lying positive parity states. It is seen that the decay of the 12_1^+, 13_1^+, 14_2^+, and 15_1^+ states is predicted reasonably well. The position of the calculated 16_1^+ state fits well with that of the observed states with possible spin 16.

For the negative parity bands, the calculations are, in general, in good agreement with the observed features. Both the signature splitting and in-band and interband decay of these states are well described (Fig. 3 and Table II). Calculations predict the first and second 14^- states with excitation energies that differ by less than 100 keV. The resulting wave

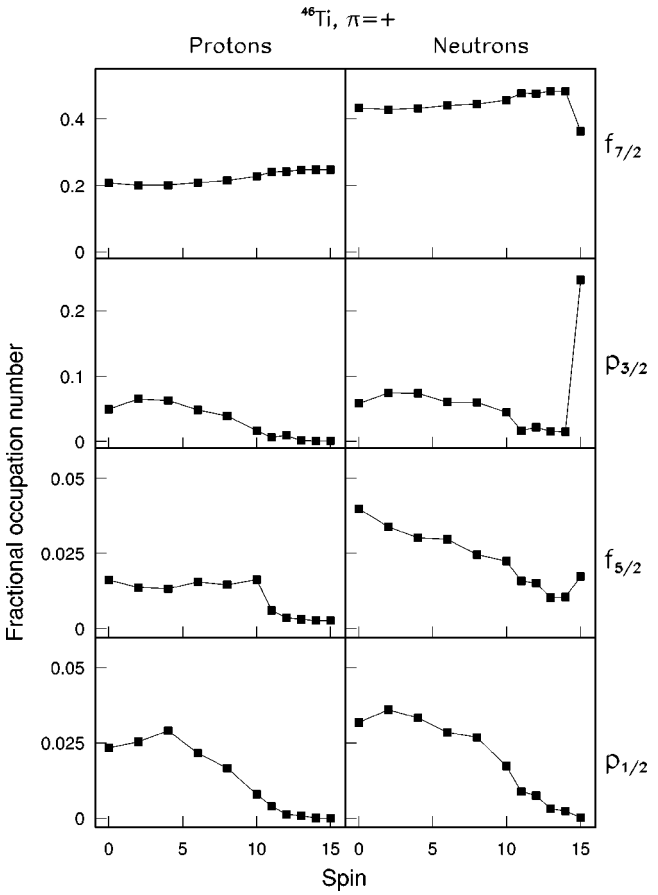

FIG. 5. Wave function components for the positive parity yrast states.

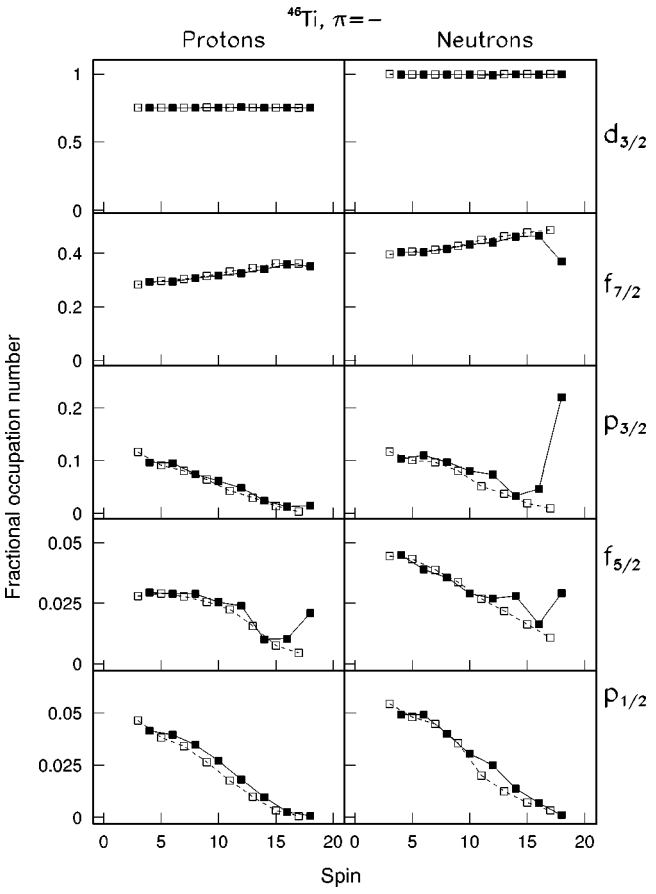

FIG. 6. Same as Fig. 5, but for the negative parity states.

functions are thus mixed and this can explain the lack of agreement for the decay of the 14_1^- and 15_1^- states in Table II. The calculations also show that the $J^\pi = 18^-$ state, above the band terminations, which fits well the position of the observed one, decays preferentially towards the terminating state of the $\alpha = 1$ band, as observed experimentally.

For the experimental states without parity assignment from Fig. 1, also shown separately in the middle of Fig. 3, it was not possible to establish unambiguous correspondences with calculated levels.

Figure 4 gives a comparison of both the positive and negative parity bands of ^{46}Ti with the rotor formula $E(J) = 0.05473J(J+1)$. In the positive yrast band, the nucleus is seen to be a reasonably good rotor up to the spin $J=8$; above that, the sudden change of the slope indicates a drastic change of configuration, which leads to gradually less collectivity. The negative parity bands have a much more regular rotational aspect (Fig. 1): the rotational character is relatively good up to spin $J=10$, after that there is again a change of slope indicating a different regime. Both changes of regime show up experimentally in a back bending. Above the maximum aligned spin, the smooth behavior is broken indicating an abrupt change of configuration.

These changes of configuration can be also followed in the structure of the wave functions. Figure 5 shows the wave function compositions (fractional shell occupations) of the yrast positive parity states. The wave functions are dominated, as expected, by the $f_{7/2}$ orbital, but the $p_{3/2}, f_{5/2}$, and $p_{1/2}$ orbitals play also some role. It is seen that these higher orbitals have a significant contribution in the structure of the states up to spin 8. This indicates a stronger collectivity of these states. As proved in previous calculations [18], it is the mixing between the $f_{7/2}$ and $p_{3/2}$ orbitals which enhances the quadrupole coherence and gives rise to rotational states. After spin 8, the contribution of all these orbitals falls practically to zero, which means that the spin is built only by aligning $f_{7/2}$ particles. This process continues up to spin 14 (fully aligned, or terminating state). At $J^\pi = 15^+$, one sees that, essentially, one $f_{7/2}$ neutron is excited into the $p_{3/2}$ orbital.

Figure 6 shows the occupation numbers for the negative parity band states (both signatures). One observes the same trend as discussed above for the positive parity states, except that here the decrease (with increasing spin) of the components due to the higher pf orbitals is more gradual up to the terminating states. This is the reason why the loss of collectivity (Fig. 4) is more gradual in this band than in the positive parity band. The 18^- state observed above the termination is again realized by promoting one $f_{7/2}$ neutron into the $p_{3/2}$ orbit.

In conclusion, in the present work, the level scheme of ^{46}Ti has been greatly expanded at high spins. We have observed for the first time γ-ray transitions above the termina-

tion of both the natural and unnatural parity bands. Shell model calculations have been performed for the full pf space allowing also particle-hole excitations from the $d_{3/2}$ orbital. These calculations describe well the experimental features and offer an insight into the microscopic origin of the observed behavior with spin. The observed bands are rather collective up to spin $\sim 8-10$, where the alignment of $f_{7/2}$ particles sets in, inducing a gradual loss of collectivity up to the terminating states. The alignment is more gradual for the unnatural parity bands giving rise to a smoother termination in this case. After the terminating states, excitation of one $f_{7/2}$ neutron into the $p_{3/2}$ orbital induces an abrupt change of the smooth behavior.

ACKNOWLEDGMENT

D.B. wishes to acknowledge support within the INFN-INFIN collaboration agreement.

[1] E. Caurier, A.P. Zuker, A. Poves, and G. Martinez-Pinedo, Phys. Rev. C **50**, 225 (1994); E. Caurier, J.L. Egido, G. Martinez-Pinedo, A. Poves, J. Retamosa, L.M. Robledo, and A.P. Zuker, Phys. Rev. Lett. **75**, 2466 (1995).

[2] S.M. Lenzi *et al.*, Z. Phys. A **354**, 117 (1996); Phys. Rev. C **56**, 1313 (1997); F. Brandolini *et al.*, Nucl. Phys. **A642**, 347 (1998); J.A. Cameron *et al.*, Phys. Lett. B **387**, 266 (1996).

[3] C.A. Ur *et al.*, in Proceedings of the International Workshop PINGST 2000 on Selected Topics on $N=Z$ Nuclei, Lund, 2000, edited by D. Rudolph and M. Hellstrom, p. 252.

[4] P. Bednarczyk, W. Meczyński, J. Styczeń, J. Grebosz, M. Lach, A. Maj, and M. Zieblíński, Acta Phys. Pol. B **32**, 747 (2001).

[5] S.M. Lenzi, D.R. Napoli, C.A. Ur, D. Bazzacco, F. Brandolini, J.A. Cameron, E. Caurier, G. de Angelis, M. De Poli, E. Farnea, A. Gadea, S. Hankonen, S. Lunardi, G. Martinez-Pinedo, Zs. Podolyak, A. Poves, C. Rossi Alvarez, J. Sánchez-Solano, and H. Somacal, Phys. Rev. C **60**, 021303(R) (1999).

[6] F. Brandolini, H.H. Medina, S.M. Lenzi, D.R. Napoli, A. Poves, R.V. Ribas, J. Sánchez-Solano, C.A. Ur, M. De Poli, N. Marginean, D. Bazzacco, J.A. Cameron, G. de Angelis, A. Gadea, R. Menegazzo, and C. Rossi Alvarez, Nucl. Phys. **A693**, 517 (2001).

[7] L.K. Peker, Nucl. Data Sheets **68**, 271 (1993).

[8] S.-C. Wu, Nucl. Data Sheets **91**, 1 (2000).

[9] A.R. Poletti, E.K. Warburton, and J.W. Olnes, Phys. Rev. C **23**, 1550 (1981).

[10] N.R.F. Rammo, P.J. Nolan, L.L. Green, A.N. James, J.F. Sharpey-Schafer, and J.M. Sheppard, J. Phys. G **8**, 101 (1982).

[11] J.A. Cameron, J.L. Rodriguez, J. Jonkman, G. Hackman, S.M. Mullins, C.E. Svensson, J.C. Waddington, Lihong Yao, T.E. Drake, M. Cromaz, J.H. DeGraaf, G. Zwarts, H.R. Andrews, G. Ball, A. Galindo-Uribarri, V.P. Janzen, D.C. Radford, and D. Ward Phys. Rev. C **58**, 808 (1998).

[12] D. Bazzacco, Proceedings of the International Conference on Nuclear Structure at High Angular Momentum, Ottawa, 1992, Vol. 2, p. 376.

[13] E. Farnea, G. de Angelis, M. De Poli, D. De Acuna, A. Gadea, D.R. Napoli, P. Spolaore, A. Buscemi, R. Zanon, R. Isocrate, D. Bazzacco, C. Rossi Alvarez, P. Pavan, A.M. Bizzeti-Sona, and P.G. Bizzeti, Nucl. Instrum. Methods Phys. Res. A **400**, 87 (1997).

[14] S.M. Lenzi, C.A. Ur, D.R. Napoli, M.A. Nagarajan, D. Bazzacco, D.M. Brink, M.A. Cardona, G. de Angelis, M. De Poli, A. Gadea, D. Hojman, S. Lunardi, N.H. Medina, and C. Rossi Alvarez, Phys. Rev. C **56**, 1313 (1997).

[15] K.S. Krane, R.M. Steffen, and R.M. Wheeler, Nucl. Data Tables **11**, 351 (1973).

[16] M. Piiparinen, A. Ataç, J. Blomqvist, G.B. Hagemann, B. Herskind, R. Julin, S. Juutinen, A. Lampinen, J. Nyberg, G. Sletten, P. Tikkanen, S. Tormanen, A. Virtanen, and R. Wyss, Nucl. Phys. **A605**, 191 (1996); N.H. Medina, F. Brandolini, D. Bazzacco, P. Pavan, C. Rossi Alvarez, R. Burch, S. Lunardi, R. Menegazzo, M. De Poli, G. Maron, R.V. Ribas, and M. Ionescu-Bujor, *ibid.* **A589**, 106 (1995).

[17] E. Caurier, computer code ANTOINE, Strasbourg, 1989.

[18] A.P. Zuker, J. Retamosa, A. Poves, and E. Caurier, Phys. Rev. C **52**, R1741 (1995).